The Structure and Phase Diagram of Langmuir Films of Alcohols on Mercury

H. Kraack,[†] B. M. Ocko,[‡] P. S. Pershan,[§] E. Sloutskin,[†] L. Tamam,[†] and M. Deutsch*,[†]

Department of Physics, Bar-Ilan University, Ramat-Gan 52900, Israel, Department of Physics, Brookhaven National Laboratory, Upton, New York 11973, and Department of Physics, Harvard University, Cambridge, Massachusetts 02138

Received January 22, 2004. In Final Form: April 2, 2004

The coverage-dependent phase behavior of molecular films of alcohols ($CH_3(CH_2)_{n-2}CH_2OH$, denoted as C*n*OH) on mercury was studied for chain lengths $8 \le n \le 28$, using surface tensiometry and surface specific X-ray methods. Phases with surface-normal-oriented molecules are found at high coverage, showing the CS, S, and LS phases found also on water. Phases comprising surface parallel molecules, which do not exist on water, are found here at low coverage. For the lowest coverage a two-dimensional gas phase is found, followed, upon increasing the coverage, by an *n*-dependent sequence of condensed phases of up to four layers of surface-parallel molecules before converting to the surface-normal phases. In contrast with the surface-normal phases, all of the surface-parallel phases are found to lack long-range order in the surface-parallel direction. Adsorption energies are derived from the phase diagram for the alkyl chain and the alcohol headgroup.

I. Introduction

Until recently, X-ray studies of Langmuir films, which allow ångström scale structure determination, employed almost exclusively aqueous subphases.[1−4] On such subphases all Langmuir-film-forming amphiphiles invariably orient along, or slightly tilted from, the surface normal due to the dominant hydrophobic repulsion between the organic tail of the molecule and the aqueous subphase. Starting from the first in situ X-ray studies of Langmuir films[5] almost two decades ago, a large variety of molecules were studied. In particular, fatty acids received the most attention and their phase diagram was determined in detail. The universality of its phase diagram upon chain length variation was demonstrated,[6] and a detailed theoretical description and interpretation of its phase diagram within a Landau-type mean-field theory was achieved.[1] The less-detailed studies of Langmuir films of alcohols on aqueous subphases presented a very similar phase behavior, showing almost the same phases as for Langmuir films of fatty acids, but with a different tilt direction: toward next-nearest neighbors[7] rather than toward nearest neighbors, as in fatty acids. This similarity stems largely from the same chain−chain interaction, which determines the structure for high coverages, and a close, though somewhat different, headgroup−subphase interaction for the two types of molecules.

To gain a better understanding of the role of the subphase in determining the structure and phase behavior of Langmuir films, studies on nonaqueous subphases are required. This, however, has been mostly neglected to date. Mercury has several advantages as a subphase for such studies. It attracts, rather than repels, the chains of organic molecules and thus does not necessarily induce surface-normal molecular orientation. Its interaction with polar and nonpolar headgroups and chains is fundamentally different from that of polar water, and of course, it does not form hydrogen bonds or hydration shells around polar or ionic headgroups. Its high surface tension (∼500 mN/m) allows for spreading Langmuir films of materials which do not spread either readily or not at all on the lower-surface-energy water. There are several additional advantages, not least among them are the very low surface roughness, ∼1 Å, due to the high surface tension and the high electron density of the mercury, $\rho = 3.25$ electrons/Å^3. This allows extending X-ray reflectivity measurements to 4-fold higher angles than those on water, yielding a commensurate increase in resolution.[8−11]

We have recently studied Langmuir films of fatty acids and alkanes on mercury.[10−13] In contrast with Langmuir films on water, the attractive chain−subphase interaction

* To whom correspondence may be addressed. E-mail: deutsch@mail.biu.ac.il.

[†] Bar-Ilan University.

[‡] Brookhaven National Laboratory.

[§] Harvard University.

(1) Kaganer, V. M.; Möhwald, H.; Dutta, P. *Rev. Mod. Phys.* **1999**, *71*, 779.

(2) Als-Nielsen, J.; Jacquemain, D.; Kjaer, K.; Leveiller, F.; Lahav, M.; Leizerrowitz, L. *Phys. Rep.* **1994**, *246*, 252.

(3) Kuzmenko, I.; Rapaport, H.; Kjaer, K.; Als-Nielsen, J.; Weissbuch, I.; Lahav, M.; Leiserowitz, L. *Chem. Rev.* **2001**, *101*, 1659.

(4) Rapaport, H.; Kuzmenko, I.; Berfeld, M.; Kjaer, K.; Als-Nielsen, J.; Popovitz-Biro, R.; Weissbuch, I.; Lahav, M.; Leiserowitz, L. *J. Phys. Chem. B* **2000**, *104*, 1399.

(5) Grayer Wolf, S.; Leiserowitz, L.; Lahav, M.; Deutsch, M.; Kjaer, K.; Als-Nielsen, J. *Nature* **1987**, *328*, 63. Kjaer, K.; Als-Nielsen, J.; Helm, C. A.; Laxhuber, L. A.; Möhwald, H. *Phys. Rev. Lett.* **1987**, *58*, 2224. Dutta, P.; Peng, J. B.; Lin, B.; Ketterson, J. B.; Prakash, M.; Georgopoulos, P.; Ehrlich, S. *Phys. Rev. Lett.* **1987**, *58*, 2228.

(6) Peterson, I. R.; Brzezinski, V.; Kenn, R. M.; Steitz, R. *Langmuir* **1992**, *8*, 2995.

(7) Shih, M. C.; Bohanon, T. M.; Mikrut, J. M.; Zschack, P.; Dutta, P. *J. Chem. Phys.* **1992**, *97*, 4485. Bohanon, T. M.; Lin, B.; Shih, M. C.; Ice, G. E.; Dutta, P. *Phys. Rev. B* **1990**, *41*, 4846.

(8) Magnussen, O. M.; Ocko, B. M.; Deutsch, M.; Regan, M. J.; Pershan, P. S.; Abernathy, D.; Grübel, G.; Legrand, J. F. *Nature* **1996**, *384*, 250.

(9) Deutsch, M.; Magnussen, O. M.; Ocko, B. M.; Regan, M. J.; Pershan, P. S. In *Thin Films*: *Self-Assembled Monolayers of Thiols*; Ulman, A., Ed.; Academic: San Diego, CA, 1998.

(10) Kraack, H.; Ocko, B. M.; Pershan, P. S.; Sloutskin, E.; Deutsch, M. *Science* **2002**, *298*, 1404.

(11) Kraack, H.; Deutsch, M.; Ocko, B. M.; Pershan, P. S. *Nucl. Instrum. Methods Phys. Res., Sect. B* **2003**, *200*, 363.

(12) Kraack, H.; Ocko, B. M.; Pershan, P. S.; Sloutskin, E.; Deutsch, M. *J. Chem. Phys.* **2003**, *119*, 10339.

(13) Kraack, H.; Ocko, B. M.; Pershan, P. S.; Sloutskin, E.; Tamam, L.; Deutsch, M. *Langmuir* **2004**, *20*, 5375.

10.1021/la0497954 CCC: $27.50
Published on Web 05/18/2004

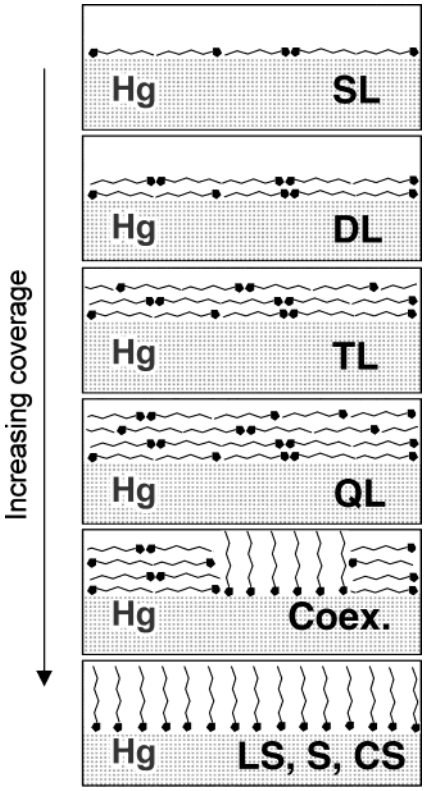

Figure 1. Real space model of C26OH on mercury, showing with increasing coverage the growth of single (SL), double (DL), triple (TL), and quadruple (QL) layer of lying down molecules, the untilted standing-up (CS, S, LS) monolayer phase, and the coexistence region (Coex.) between the lying-down and the standing-up phases.

on mercury induces phases where the molecules are oriented parallel to the surface at low coverages and are either ordered (fatty acids) or disordered (alkanes) in the surface-parallel direction. At higher surface pressures the fatty acid films transform to phases of molecules aligned along the surface normal, while alkanes on mercury do not show standing-up phases at all. The in-plane order in fatty acids consists of ordered molecular dimers. This phase behavior is different from that of Langmuir films on water, where fatty acids show only surface-normal phases, and alkanes are found to form macroscopic multilayer crystallites comprising highly tilted molecules.[3,14]

We present here a study of *n*-alcohols on mercury, using surface pressure vs area isotherms, and surface specific X-ray diffraction. Depending on chain length, up to four different lying-down phases are found having one, two, three, and four molecular layers. In contrast, the maximum number of lying-down layers for alkanes or fatty acids is three. A schematic view of the phase sequence for increasing coverage is shown in Figure 1: the single (SL), double (DL), triple (TL) and quadruple (QL) lying-down phases, the untilted standing-up (CS) phase, and the coexistence region (Coex.) between the standing-up and lying-down phases. The standing-up phases of *n*-alcohols are found to be similar to those on water, but with the tilted phases suppressed. The phase diagram is determined, and from this the adsorption energies on mercury of the alkyl chain and the alcohol headgroup are determined. The later is found to be surprisingly close to, though somewhat smaller than, that of fatty acids on mercury.

(14) Weinbach, S. P.; Weissbuch, I.; Kjaer, K.; Bouwman, W. G.; Als-Nielsen, J.; Lahav, M.; Leiserowitz, L. *Adv. Mater.* **1995**, *7*, 857.

II. Experiment

The methods and equipment used are identical with those in previous publications[11−13] and will be described here only briefly.

A specially designed Langmuir trough, suitable for simultaneous film balance and X-ray studies, was used for the experiments. Measurements were carried out under inert He (X-ray) or nitrogen (surface tensiometry) atmosphere. The temperature of the mercury is controllable by a water circulation system to ±0.2 °C.

The surface tension measurements employed the Wilhelmy plate method[15] with an Hg-amalgamated platinum plate, hanging off a leaf spring. Its position, which is proportional to the surface tension, was measured using a linear variable differential transformer (LVDT).[11,12]

Mercury was purchased from Merck Co. (triple distilled, 99.999 pure) and from Bethlehem Apparatus Co. (quadruple distilled 99.99995% pure). The alcohols were purchased from Fluka, Sigma, or Aldrich and were at least 98% pure. All materials were used as received. No variations were found in our results upon using mercury and/or alcohols from a different manufacturer or of slightly different purities. Standard solutions of molarities $(3-8) \times 10^{-4}$ in HPLC grade, 99.9% pure chloroform (Aldrich) were used. The films were deposited stepwise, using a micropipet, through a resealable hole in the trough's enclosure.

III. Measurement Methods

A. Surface Pressure−Molecular Area Isotherms. The surface pressure, $\pi = \sigma_0 - \sigma$, where σ_0 and σ are the surface tensions of the bare and film-covered liquid surface, respectively, varies with the surface coverage, given by the area per molecule A.[15] The π vs A curve, the isotherm, hints at the molecular structure of the Langmuir film and provides indications for the nature of the phases, transitions between them, etc.

As in earlier experiments, the trough was cleaned carefully, and then its enclosure was flushed with a pure inert gas (He or N_2) for about 1 h. Mercury was introduced through a capillary tube from a reservoir. The isotherm was then measured by stepwise deposition by a micropipet of an amount of the standard solution, waiting after each step until an equilibrium pressure was reached.

B. X-ray Measurements. The molecular-level structure of the Langmuir films was studied at various coverages using surface specific X-ray techniques. The X-ray measurements were carried out at the Harvard/BNL liquid surface spectrometer at beamline X22B, NSLS, Brookhaven National Laboratory, at wavelengths of $\lambda = 1.53-1.58$ Å. The trough was supported on an active vibration isolation unit, mounted on the spectrometer.[16] This arrangement was demonstrated in previous measurements[8,10,17] to eliminate vibrational pickup from the environment, the major cause of the strongly limited range and low data quality achieved in early studies of the surface structure of mercury.[18]

A detailed description of the X-ray measurement methods used and the modeling by a box-model are available in the literature[1,2,12,19] and will not be repeated here. We have carried out X-ray reflectivity (XR) measurements, which yield information on the surface-normal

(15) Gaines, G. L. *Insoluble Monolayers at Liquid−Gas Interfaces*; Wiley-Interscience: New York, 1966.

(16) Braslau, A.; Pershan, P. S.; Swislow, G.; Ocko, B. M.; Als-Nielsen, J. *Phys. Rev. A* **1988** *38*, 2457.

(17) Magnussen, O. M.; Ocko, B. M.; Regan, M. J.; Penanen, K.; Pershan, P. S.; Deutsch, M. *Phys. Rev. Lett.* **1995**, *74*, 4444. Dimasi, E.; Tostmann, H.; Ocko, B. M.; Pershan, P. S.; Deutsch, M. *Phys. Rev. B* **1998**, *58*, 13419.

(18) Barton, S. W.; Thomas, B. N.; Novak, F.; Weber, P. M.; Harris, J.; Dolmer, P.; Bloch, J. M.; Rice, S. A. *Nature* **1986**, *321*, 685. Lu, B. C.; Rice, S. A. *J. Chem. Phys.* **1978**, *68*, 5558. Bosio, L.; Oumezine, M. *J. Chem. Phys.* **1984**, *80*, 959. Bosio, L.; Cortes, R.; Folcher, G.; Froment, M. *J. Electrochem. Soc.* **1992**, *139*, 2110.

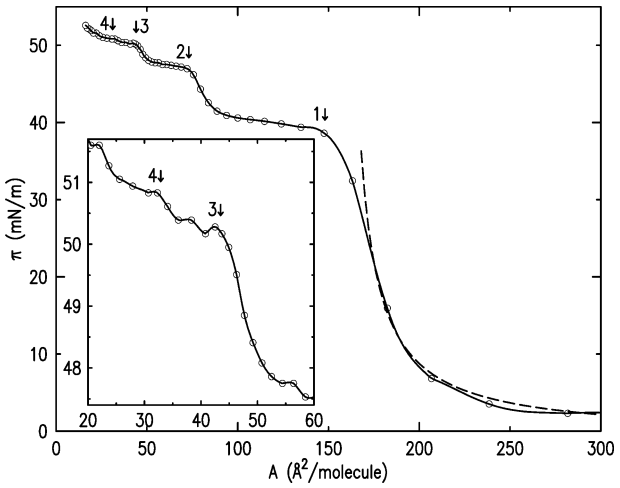

Figure 2. Measured surface pressure π vs area A isotherms (T = 23 °C) for C26OH (points + solid line) and its fit by the Volmer equation (dash line), yielding an exclusion area of 157 Å^2/molecule. The layer by layer growth of the lying-down phases can be clearly observed by the formation of successively higher plateaus in the isotherm. The onsets of these plateaus are marked by numbered arrows. The inset shows the onset of the fourth (short) plateau on an enlarged scale.

structure of the Langmuir film such as its surface-normal electron density profile and its surface roughness. The in-plane order was investigated by grazing incidence diffraction (GID). The XR measurements employed a NaI point detector while the GID was measured using a position-sensitive detector, aligned within the vertical scattering plane, which allows the simultaneous measurement of a full Bragg rod (BR) at the positions where GID peaks are observed. To minimize beam damage, exposure times of the sample were kept to the necessary minimum by using an automatic shutter upstream of the trough. This was only open during the time of the measurement.

IV. Results and Discussion

We present first (A, π) isotherms for $8 \le n \le 28$, and X-ray data for n = 14, 18, 22, and 26. This is followed by an intercomparison of the results for the different chain lengths and a discussion of the resultant phase diagram. Finally, we will discuss the alcohol results in comparison with our previous studies of fatty acids and alkanes on mercury.[12,13]

A. Isotherms. Figure 2 shows the isotherm of C26OH, taken at T = 23 °C. The measured points are shown by open circles. These are connected by a smoothed line. One obvious disadvantage of the stepwise addition of material is that the size of the areal step due to the addition of even a minimal amount of solution is very large at low coverages. Thus, we have only a small number of points at low coverages. For $A \ge 220$ Å^2/molecule, the surface pressure does not increase significantly with decreasing A. With further decrease in the area, the pressure starts to show a strong increase which levels off at a pressure of 40 mN/m and an area of A = 160 Å^2/molecule. The increase in the surface pressure can be reasonably well fitted by the Volmer equation, $\pi(A - A_1) = kT$ (dashed line), the ideal gas law in two dimensions, with an exclusion area A_1 = 157 Å^2/molecule. Employing lengths of 1.27, 1.5, and 2.4 Å for the C−C bond projected on the molecular axis, and the van der Waals radii of the CH_3 and CHOH groups, respectively,[20,21] as well as a width of 4.3 Å derived in the X-ray measurements discussed below for the thickness of a flat-lying alcohol molecule, the calculated area occupied by a single lying-down molecule is 153 Å^2, in good agreement with the exclusion area A_1. As discussed in an accompanying publication,[13] the association of the exclusion area obtained from a fit by the Volmer equation with the geometrical area occupied by a molecule originates in the work of Langmuir[22] and is further supported by a number of subsequent theoretical and experimental studies.[23] We use the Volmer equation (and not, e.g., the van der Waals one, see ref 13) only to demonstrate that the bend in the isotherm at A_1 is due to the formation of a closely packed layer of flat-lying molecules.

Below A_1 two additional plateaus are formed at coverages of 79 and 47 Å^2/molecule and surface pressures of 48 and 51 mN/m, respectively. The onsets of the three plateaus are marked by numbered arrows 1 to 3 in Figure 2. The fact that the second plateau is formed at one-half the area/molecule of the first plateau points toward the formation of a double layer, as was also found for fatty acids and alkanes of various chain lengths.[12,13] The onset area of the third plateau is close to, though somewhat below, one-third of A_1 indicating that a triple layer is formed. On an enlarged scale, shown in the inset to Figure 2, a small, barely significant, jump can be observed at ~34 Å^2/molecule, marked by arrow 4. This, again, is close to, though somewhat smaller than, one-quarter of A_1. If this jump is indeed real, it could indicate the formation of a quadruple layer of flat-lying molecules. We will return to this point in section B below and show that the X-ray measurements indeed reveal the existence of such a quadruple layer.

The (A, π) isotherms of alcohols of other chain lengths, $8 \le n \le 28$, measured all at T = 23 °C, are shown in Figure 3. For clarity the isotherms of C18OH, C22OH, C26OH, and C28OH are shifted by π = 5 mN/m from each other. The various plateau onsets, the corresponding pressures, and the collapse pressure of each of the alcohols measured are summarized in Table 1.

We observe three qualitatively different behaviors in the isotherms, depending on chain length. For $22 \le n \le 26$ we observe the formation of three clear plateaus as described above in detail for C26OH, which is the only molecule which shows also a possible fourth plateau. For $14 \le n \le 18$, and also for C28OH, two plateaus are observed and for $n \le 12$, only a single plateau. The areas per molecule at the onset of the plateaus are plotted as a function of chain length in Figure 4. All onset areas are observed to increase linearly with chain length: $A_1 = (6 \pm 6) + (6.1 \pm 0.2)n$ Å^2/molecule, $A_2 = (3 \pm 3) + (2.9 \pm 0.2)n$ Å^2/molecule, and $A_3 = (2 \pm 2) + (1.7 \pm 0.2)n$ Å^2/molecule. The last two are very close to $A_1/2$ and $A_1/3$, respectively. The only deviation from linearity is in A_1 for C8OH. The lower than expected value of A_1 for C8OH may indicate that a large number of molecules prefer to stand up already before completion of a single layer of lying down molecules.

(19) Deutsch, M.; Ocko, B. M. In *Encyclopedia of Applied Physics*; Trigg, G. L., Eds.; VCH: New York, 1998; Vol. 23, p 479. Als-Nielsen, J.; McMorrow, D. In *Elements of Modern X-ray Physics*; Wiley: New York, 2001.

(20) Small, D. M. In *The Physical Chemistry of Lipids*; Plenum: New York, 1986.

(21) Israelachvili, J. In *Intermolecular and surface forces*; Academic: London, 1992.

(22) Langmuir, I. *J. Am. Chem. Soc.* **1932**, *54*, 2798. See also the discussion of the exclusion area of docosane on mercury in ref 12.

(23) Israelachvilli, J. *Langmuir* **1994**, *10*, 3774. Fainerman, V. B.; Volhardt, D. *J. Phys. Chem. B* **2003**, *107*, 3098. Tonks, L. Private communication, cited in ref 22. Vollhardt, D.; Fainerman, V. *Colloids Surf., A* **2001**, *176*, 117. Langmuir, I. *J. Chem. Phys.* **1933**, *1*, 756. Davies, J. T. *Proc. R. Soc. London, Ser. A* **1951**, *208*, 224. Phillips, J. N.; Rideal, E. *Proc. R. Soc. London, Ser. A* **1955,** *232*, 149.

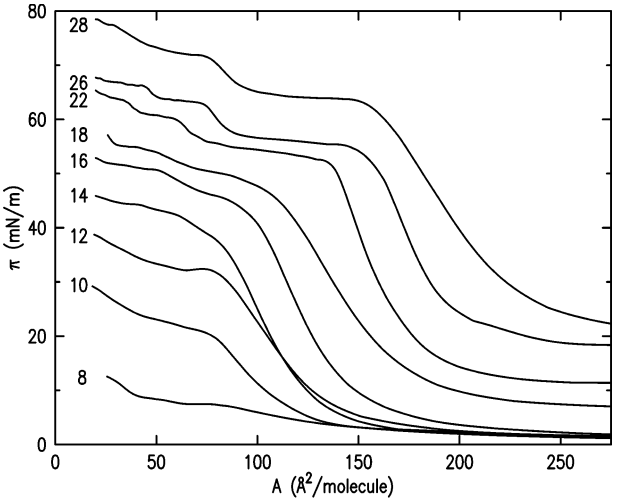

Figure 3. (A,π) isotherms for alcohol molecules of chain lengths $8 \le n \le 28$. The isotherms of C18OH, C22OH, C26OH, and C28OH are upshifted by $\pi = 5$, 10, 15, 20 mN/m, respectively.

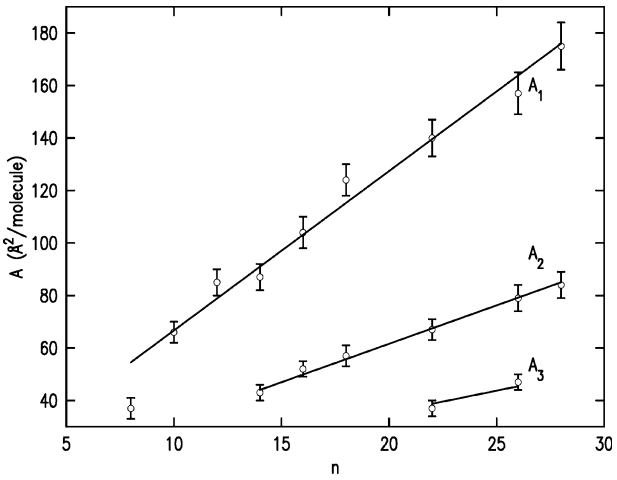

Figure 4. Exclusion area values A_1 obtained from fits of the Volmer equation to the isotherms and onset areas of the second, A_2, and third, A_3, plateaus of the isotherms in Figure 2 (points), with their linear fits (lines). The second plateau is observed only for $n \ge 14$, and the third plateau only for $22 \le n \le 26$.

Table 1. Fitted Exclusion Area, A_1, and Onset Areas of the Second, A_2, and Third, A_3, Plateaus, with Their Corresponding Surface Pressures π_1, π_2, and π_3, and the Collapse Pressure π_c for Different Chain Length Alcohols C_nOH[a]

	Å²/molecule			mN/m			
n	A_1	A_2	A_3	π_1	π_2	π_3	π_c
8	37(5)			7			16
10	66(4)			21			30
12	85(5)			32			40
14	87(5)	43(4)		38	44		46
16	104(6)	52(4)		42	51		53
18	124(6)	57(5)		42	50		53
22	140(7)	67(5)	37(4)	42	49	52	54
26	157(8)	79(5)	47(4)	40	48	51	54
28	175(9)	84(5)		44	52		59

[a] The numbers in parentheses are the uncertainties in the last digit of the quoted value.

A similar effect was observed for short-chain fatty acids and can be assigned to the lower gain in energy for a lying-down molecule (which has a better chain−mercury contact) over a standing-up one (which has a better headgroup−mercury contact) because of the short chain length.[13]

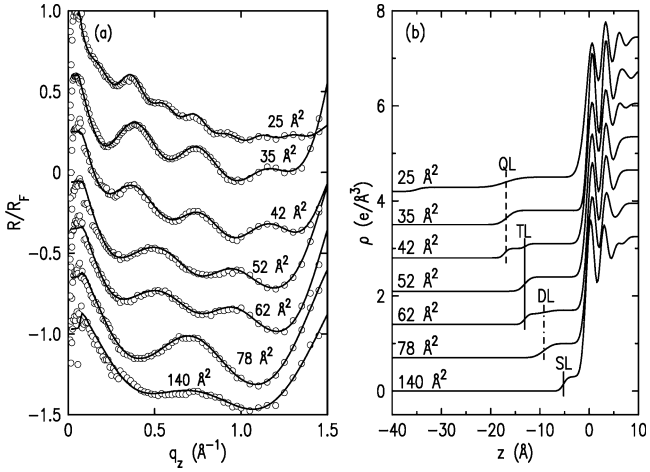

Figure 5. (a) Measured (points) and box model fitted (lines) X-ray reflectivities for C26OH on mercury at the indicated coverages. (b) The electron densities derived from the fits. The XRs show from bottom to top the successive growth of four layers of lying-down molecules and the coexistence between standing-up and lying-down molecules at 25 Å²/molecule. No pure, standing-up-only phase could be obtained at room temperature by just increasing the coverage.

The isotherms for the shorter chains are different. Starting at $n = 12$, with decreasing n we observe a single distinct plateau for $A < A_1$ that becomes progressively less horizontal. The isotherms show also a more rounded bend at A_1 and a lower pressure π for the plateau with decreasing n. This indicates an increasingly incomplete coverage of the single layer of flat lying molecules as n decreases with an eventual disappearance of the single flat-lying phase for C7OH and shorter molecules. Qualitatively the isotherms are very similar to and show the same features as those of fatty acids on mercury.[13] This includes the sharp increase at areas slightly larger than the exclusion area A_1, for most chain lengths the same number of plateaus and a similar surface pressure at the plateaus. Both classes of molecules show a small pressure increase toward small areas, which indicates compressed phases of standing up molecules. Aside from this small increase the isotherms of alcohols resemble also those taken for alkanes on mercury.[12]

B. X-ray Measurements. In this section we describe the X-ray reflectivity and grazing incident diffraction results for C14OH, C18OH, C22OH, and C26OH. All reflectivities were taken at $T = 25$ °C, while for the grazing incidence diffraction we varied the temperatures over a wide temperature range. The results for C22OH and C26OH exhibit a phase behavior which encompasses the entire range of phenomena observed; therefore we first highlight these results. Moreover, C22OH is an attractive molecule to study since it has been extensively investigated on aqueous subphases, and it also exhibits the richest phase diagram at temperatures close to, and slightly below, room temperature. The comparison with the water-supported film should be relevant to the standing-up phases of our films. Mercury-supported C26OH films exhibit, however, the largest overall number of plateaus, as discussed in the previous section, and shows, therefore, the richest phase diagram for the lying-down phases.

1. X-ray Reflectivity. Figure 5a shows a set of Fresnel-divided reflectivities measured (points) for C26OH at the indicated areas per molecule as calculated from the amount of material deposited. These curves were taken at positions along the isotherm corresponding to the lying down single, double, triple, quadruple layers and the standing up layer regimes. The range of q_z measured does

Table 2. Nominal Coverage (A), Layer Thickness (d), Phase, Fractional Coverage of the Topmost Layer in % (Top), and the Roughnesses of the Alcohol−Air (σ_{Alc}) and the Mercury−Alcohol (σ_{Hg}) Interfaces, As Obtained from Fits to the XR Curves in Figure 5 for a C26OH Layer at T = 25 °C

A, Å^2	d, Å	phase	top, %	σ_{Alc}, Å	σ_{Hg}, Å
140	4.7	SL	100	0.9	0.9
78	9.1	DL	100	1.5	1.0
62	13.1	TL	70	1.1	1.1
52	13.1	TL	100	1.0	1.0
42	17.2	QL	65	0.9	1.1
35	16.9	QL	100	1.3	0.9
25	34.9	CS	30	1.5	1.4

not extend to the layering peak of the mercury, $q_z = 2.3$ Å^{-1}. Fits, obtained from model density profiles, are shown as solid lines in Figure 5a and the corresponding density profiles are shown in Figure 5b. The density is modeled as a finite number of boxes, each with its own density, thickness, and roughness. Further details can be found in refs 11, 12, and 13. Thus, only a short description will be given here.

The electron density profile shows the mercury/alcohol interface at $z = 0$ and the Langmuir film at negative z values. All fits show a layering of the mercury, which is discussed in detail in the literature.[17] To approximate the known layered mercury profile[17] by a simple model, we fitted the electron density profile of the mercury by a box model with a fixed box width of 1.3 Å, a varying electron density for each box, and a fixed interbox interfacial roughness of 0.7 Å. This resulted in the oscillatory electron density shown in Figure 5b. Following an extensive set of fits with different combinations of free and fixed parameters, we employed in the fits shown here a fixed electron density of 5.5 electrons/Å^3 for the first mercury box in all fits. All roughness values obtained in the fit for the mercury−alcohol and the alcohol−air interfaces range from 0.9 to 1.3 Å, close to those of a pure mercury surface. The electron densities of the alcohols are also modeled by boxes. Fitting the electron density of the lying-down phases as well as the alkyl chains of the standing-up phases freely resulted in electron densities of $0.26 \le \rho \le 0.34$ electrons/Å^3. Thereafter a density of $\rho = 0.30$ electrons/Å^3 was used for the lying-down phases as well as for the alkyl chains of the standing-up phases to have better comparison between different fits and to minimize the number of fit parameters. In the standing-up phases, the electron density and length of the alcohol headgroup were held constant at 0.40 electrons/Å^3 and 2.0 Å, respectively, since for such thin layers these two parameters are highly correlated when allowed to vary freely. These values were chosen to reproduce the extension of and total number of electrons in the headgroup. The thicknesses of the other boxes were allowed to vary in the fits.

The fit results, shown in lines in Figure 5a, are summarized in Table 2, and the corresponding electron density profiles are shown in Figure 5b. In the case of a partial coverage of the top layer, incoherent scattering from the different-coverage domains was assumed. The measured reflectivity was, therefore, fitted by the sum of the model *intensities* (rather than amplitudes) reflected from the two type of domains. The resultant intensity ratio of the two terms yielded the coverage of the top layer. The thickness of the standing-up monolayer is equal to the length of an extended molecule and indicates, therefore, a standing-up phase of untilted molecules. The question of a possible molecular tilt of this phase is discussed below along with those of the other alcohols studied here. The layer by layer growth indicated by the

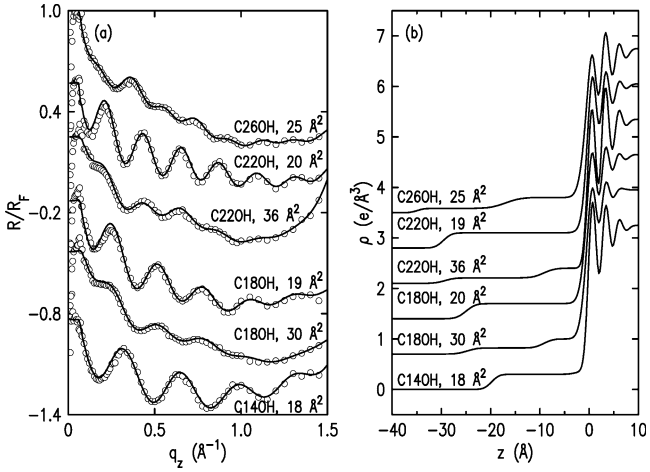

Figure 6. (a) Fresnel-normalized measured (circles) XR curves of the standing-up phases of C14OH, C18OH, C22OH, and C26OH on mercury at the indicated areas per molecule and T = 25 °C. Model fits (lines) yield the electron density profiles shown in (b).

jumps in the isotherm is clearly observed in the X-ray reflectivity results. The average layer thickness for each layer is about $d = 4.3$ Å. The third and fourth layer seem to be thinner than the first two layers, indicating perhaps a stronger attraction between the chains in these layers and those in the underlying layers, which reduces the layer spacing. The thinner upper layers might also indicate a penetration of the molecules of the upper layers into the lower layers.

The X-ray results confirm that the first, highest A, plateau in the isotherm (cf. the C26OH isotherm in Figure 1) is due to the filling up of the second lying-down layer, the first having been completed at the strong bend in the isotherm at A_1. The second layer is completed at the onset of the second plateau at 79 Å^2/molecule. The X-ray results also show that the following plateau is due to the filling up of the third lying-down layer, which is completed at the onset of the third plateau at 47 Å^2/molecule. The X-ray measurements confirm that the next plateau is indeed due to the filling-up of the fourth flat-lying layer, as suggested in the discussion of Figure 2 above. Thus, the small jump at $A \approx 34$ Å^2/molecule (arrow 4 in Figure 2) indicates the completion of the fourth layer, and onset of the coexistence region between lying-down and standing-up molecules, as indeed demonstrated by the X-ray results for 25 Å^2/molecule. The standing-up phases of C26OH observed for $A < 25$ Å^2/molecule are discussed in the following paragraph together with alcohols of other chain lengths.

Figure 6a shows a selection of reflectivity curves for C14OH, C18OH, C22OH, and C26OH at $T = 25$ °C in the high coverage regime where the standing-up phases are present. Reflectivity curves were also acquired for C14OH, C18OH, and C22OH in the lying-down single and double layer phases, but since these curves are essentially identical to those of C26OH, these curves have not been displayed. In Figure 6a, the solid lines are fits as described above and the corresponding density profiles are shown in Figure 6b.

In the bottom curve of Figure 6a we show the reflectivity for C14OH at $A = 18$ Å^2/molecule. The fitted thickness, 19.8 Å, corresponds to a standing-up monolayer. For the other chain lengths, the fitted thicknesses are 24.9 Å for C18OH, 29.5 Å for C22OH, and as previously mentioned 34.9 Å for C26OH. No differences were found in the fitted layer thickness of the standing-up monolayer in coexist-

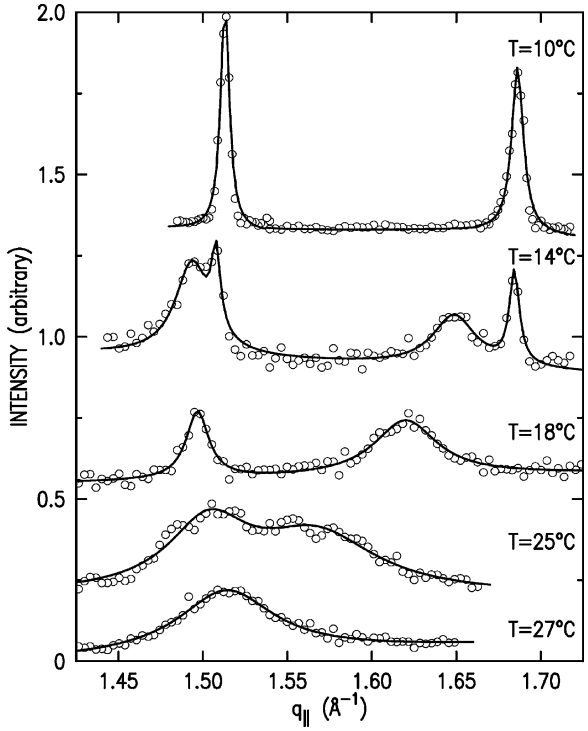

Figure 7. Measured GID patterns of the standing-up phases of C22OH at high coverage (~19 Å^2/molecule) for several temperatures, showing the transition from CS to S to LS phases with increasing temperature.

ence with the lying-down phases from that found for the full-coverage, standing-up-monolayer-only. This indicates the absence of tilted phases that are observed for Langmuir films of alcohols on water.[7] It also supports the conclusion that the standing-up phase (and by implication also the lying-down phase) is an island phase, as depicted in the panel denoted "Coex." in Figure 1. We discuss this point further in the next section dealing with the GID and BR results.

2. Grazing Incidence Diffraction. Measurements of the lateral structure of the Langmuir monolayers were carried out using GID and BR for C14OH, C18OH, C22OH, and C26OH at a range of temperatures and pressures corresponding to the lying-down and the standing-up phases. First we focus on the results for C22OH since it shows the widest range of phases near room temperature. Second, we discuss the behavior of C26OH, which shows similar behavior, except for the absence of one phase. Finally, we show the results for C14OH and C18OH, which show less temperature dependence. Before discussion of the lying-down phases, for which no long- or medium-range in-plane order is observed, the results for the standing-up phases are presented. The GID results shown for the pure standing-up phases were all measured at a high coverage, $A \approx 19$ Å^2/molecule, as calculated from the amount of material deposited. Measurements at the lower coverage coexistence range between the standing-up and the lying-down phases showed initially the same X-ray diffraction pattern as for the pure standing-up phases, but the diffraction peaks deteriorated quickly due to beam damage, exhibiting progressively lower intensities, larger peak widths, and lower $q_{||}$ positions.

Temperature-dependent GID patterns for the standing-up phases of C22OH are shown in Figure 7 (circles). The measured diffraction pattern is fitted by two Lorentzian peaks (line) on a linear background. Peak positions and widths, the corresponding lattice constants of the centered rectangular unit cell, and the area per molecule of C22OH

Table 3. Peak Positions ($q_{||}$) and Widths (fwhm), the Lattice Constants (a,b) of the Corresponding Body-Centered Rectangular Unit Cell, and the Area per Molecule (A) Calculated from the GID Measurements of C22OH at the Temperatures Indicated

T, °C	$q_{||}(11)$, Å^{-1}	fwhm, Å^{-1}	$q_{||}(02)$, Å^{-1}	fwhm, Å^{-1}	a, Å	b, Å	A, Å^2
5	1.512	0.008	1.692	0.006	5.01	7.43	18.6
10	1.513	0.006	1.686	0.008	5.00	7.45	18.6
13	1.510	0.006	1.682	0.007	5.01	7.47	18.7
14	1.508	0.006	1.684	0.007	5.02	7.46	18.7
13	1.504	0.012	1.663	0.047	5.01	7.56	18.9
14	1.494	0.024	1.649	0.031	5.04	7.62	19.2
16	1.498	0.012	1.631	0.035	5.00	7.70	19.3
18	1.497	0.016	1.620	0.045	4.99	7.76	19.4
21	1.495	0.027	1.616	0.045	5.00	7.78	19.5
25	1.503	0.058	1.567	0.086	4.90	8.02	19.6
27	1.514	0.069	1.514	0.069	4.79	8.30	19.9

obtained from the measurements are summarized in Table 3 and plotted in Figure 8. Three different phases can be distinguished clearly. For $T = 10$ °C we observe two resolution-limited diffraction peaks at $q_{||} = 1.512$ Å^{-1} and at $q_{||} = 1.686$ Å^{-1}. By use of the information of the structure of Langmuir films of long chain alcohols on water[1,7] and of fatty acid molecules on mercury,[13] the GID pattern strongly indicates a body-centered rectangular unit cell containing two molecules, with the diffraction peaks indexed as (11) and (02). The very high density of the film, 18.6 Å^2/molecule, and the resolution limited diffraction peaks in the GID, which yield a very large crystalline coherence length exceeding 1000 Å, indicate that the packing of the molecules must be herringbone-like, as is often observed for high-density Langmuir films of large chain lengths at low temperatures.[1] These structural details identify this phase as the CS phase, found also for the same alcohol monolayer on water at similar densities and temperatures.[1] For $T = 14$ °C we observe four diffraction peaks, consisting of two pairs of peaks. Two peaks are practically at the same $q_{||}$ position and have the same fitted full width at half-maximum (fwhm) as for the lower temperature, indicating that they originate in the CS phase. The two other peaks appear at slightly lower $q_{||}$ values and are significantly broader. This pattern can be interpreted as originating in two coexisting phases: a CS phase and an S phase.[1] The S phase is characterized by a slightly lower molecular density than the CS phase and different coherence lengths in different crystalline directions. At $T = 18$ °C only the peaks of the S phase are observed, indicating the end of the coexistence region. As the temperature is increased, the diffraction peaks of the S phase approach each other continuously (another signature of the S phase), become broader, and finally merge into a single peak at $T = 27$ °C. This last phase can be interpreted as a hexatic LS phase, where the hexagonal packing results in the (11) and (02) peaks having the same $q_{||}$. Further details on the structural characteristics of the CS, S, and LS phases can be found in ref 1.

These phases, their sequence and phase boundaries, correspond closely to those found for highly compressed films of C21OH on water.[7] The only difference is that the T boundaries of the phases are shifted up by ~4 °C. A similar shift is expected for our C22OH sample, which is one carbon longer.[6]

Starting with the CS phase we observe the same lattice constants as for C21OH on water (5.01 × 7.43 Å^2) at $T =$ 5 °C.[7] As typical for the CS phase the lattice expansion is almost exclusively in the longer, b, direction. Its magnitude, $(db/dT)/b = (5 \pm 1) \times 10^{-4}$ °C^{-1}, is small, corresponding to a crystalline phase rather than a rotator phase, as expected for a herringbone-ordered CS phase.

The transition to the S phase is characterized by a considerable broadening of the GID peaks, especially the (02) peak. This indicates a concomitant decrease in the crystalline coherence length from over 1000 Å in the CS phase to 400 Å ((11) direction) and 150 Å ((01) direction) in the S phase. The transition is also accompanied by a rather large increase in the area per molecule, from ∼18.7 to ∼19.2 Å^2/molecule, and in the linear expansion coefficient in the *b* direction, by almost an order of magnitude to $(db/dT)/b = (4 \pm 0.4) \times 10^{-3}$ °C^{-1}, which is similar to that of a rotator phase. The transition from the CS to the S phase shows a small jump in the lattice constants, a large decrease in the crystalline coherence length, and a small (∼1 °C) temperature range of coexistence between the two phases, all of which are indicative of a first-order transition. The main feature of the transition from the S to the LS phase is the change in symmetry; from a body-centered rectangular S phase to a hexagonal LS phase. The transition is also accompanied by a further decrease in the crystalline coherence length, with the higher value in the (11) direction approaching the lower value in the (01) direction, and by an increase in the area per molecule from 19.5 to 19.9 Å^2/molecule.

We wish to point out not only the close similarity of these structures to those of Langmuir films of alcohols on water but also the close similarity between the herringbone-structured crystalline CS phase and the orthorhombic β-phase of *bulk* alcohols. For C22OH this bulk phase has a unit cell of dimensions (5.02 × 7.43 × 121.5 Å^3), containing eight molecules.[20] In the (*a*,*b*) plane this cell has the same symmetry and dimensions as the in-plane two-dimensional (2D) unit cell of mercury- and water-supported alcohol monolayers. The only difference is a slight elongation of the bulk unit cell in the *z* direction, most likely due to hydrogen bonding in the bulk unit cell which contains eight molecules rather than the two in mercury- and water-supported monolayers. Another striking similarity exists between the hexatic LS phase and the α-phase of bulk alcohols. This phase appears in the bulk over a narrow temperature range below the freezing point. It has also an hexagonal packing with four molecules, and its dimensions are 4.85 × 8.40 × 60.0 Å^3,[20] as compared to the values of 4.79 × 8.30 × 29.5 Å^3 that are listed in the last line of Table 3.

The GID measurements for C26OH are shown in Figure 9; they present a behavior similar to that of C22OH, with one remarkable difference. The S phase, which extends over a temperature range of ∼12 °C for C22OH is not observed in C26OH. The CS phase transforms directly into the hexagonal LS phase at 36.5 ± 1.5 °C. The CS phase appears identical to that of C22OH with the temperature-independent lattice parameter $a = 5.00$ Å and a lattice parameter *b* varying linearly from $b = 7.45$ Å for $T = 13.4$ °C to $b = 7.54$ Å for $T = 34.5$ °C. As for C22OH, this corresponds to a linear lattice expansion coefficient of $(db/dT)/b = (5 \pm 0.5) \times 10^{-4}$ °C^{-1}. The LS phase of C26OH shows two significant differences relative to the LS phase of C22OH. The first is an increase in the area of the unit cell, from 19.9 to 20.3 Å^2/molecule. This may well be due to the higher transition temperature to the LS phase in C26OH, as compared to C22OH. The second difference is the peak width, which is fwhm = 0.020 Å^{-1}, three times smaller than for C22OH, leading to a crystalline coherence length of ∼300 Å, three times larger than the 100 Å found for C22OH just above the transition. This may result from the fact that the relevant measurement was carried out for C26OH on a standing-up phase in coexistence with a lying-down quadruple phase, while for C22OH the measurement was done on a pure standing-up monolayer phase. For C26OH the quadruple layer exerts a large pressure on the monolayer and thus is expected to strongly reduce the number of lattice defects in the LS phase. The lying-down phase most probably plays also a significant role in suppressing the S phase for

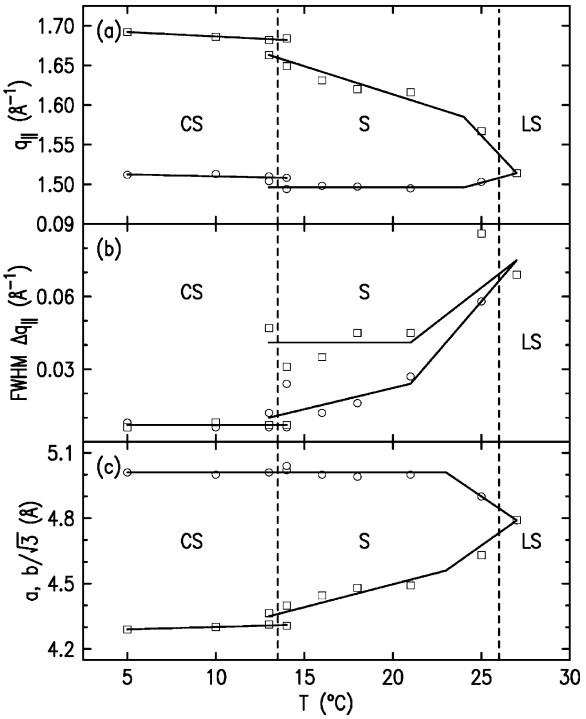

Figure 8. The temperature dependence of (a) the peak positions ($q_{||}$), (b) the peak widths (fwhm $\Delta q_{||}$), and (c) the lattice parameters (*a*, *b*) of the body-centered rectangular unit cell of C22OH. The vertical dashed lines indicate the T-boundaries of the CS, S, and LS phases, as discussed in the text.

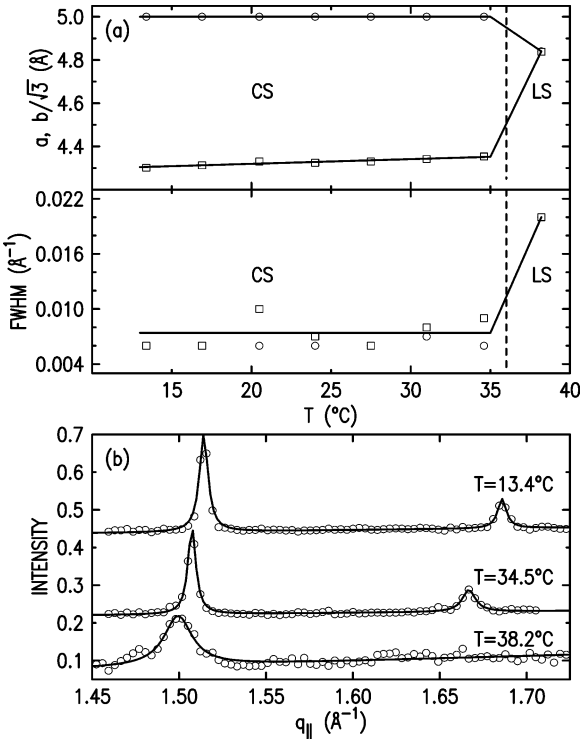

Figure 9. The temperature-dependent (a) phase behavior and (b) GID pattern for the standing-up phases of C26OH. Note the direct transition from the CS to the LS phase, in contrast with the C22OH, where an S phase is found to intrude between these two phases.

C26OH. For that phase one observes in C22OH large differences in the crystalline coherence lengths in the two lattice directions and a large continuous expansion of the unit cell, as discussed above.

For C14OH and C18OH close to, and slightly below, room temperature, we observed only a single diffraction peak, indicating a hexagonal LS phase. For C18OH at $T = 25$ °C the peak position is at $q_{||} = 1.510$ Å^{-1} and the fwhm = 0.03 Å^{-1}. For C14OH at $T = 4.5$ °C, we observe also a single GID peak at $q_{||} = 1.521$ Å^{-1} and a fwhm = 0.04 Å^{-1}. We conclude therefore that for these alcohols only the hexagonal LS phase is observed over the temperature range studied here. The crystalline coherence lengths are of order 150−200 Å.

In contrast with the high coverage phases of alcohols, which show in-plane long-range order, no sharp diffraction peaks were found for the lying-down phases of the alcohols, indicating that all lying-down phases lack long-range order. For the quadruple layer of C26OH only, we observed sometimes a weak and broad diffraction peak at $q_{||} \approx 1.29$ Å^{-1}, which was very extended in q_z. This peak corresponds to a chain−chain spacing of 4.87 Å and its width results in a liquidlike coherence length of ∼15 Å. Beam damage caused the rapid disappearance of this peak and prohibited its precise recording. It is plausible that a similar-range order exists also for a smaller number of lying-down layers. However, the smaller number of scatterers and the higher susceptibility to beam damage would render the observation of the broad liquidlike peak associated with this order increasingly more difficult with decreasing number of layers. The lack of long-range order here is similar to that found for the lying-down phases of alkanes on mercury[12] but is in contrast with the several ordered phases found for the lying-down phases of Langmuir films of fatty acids on mercury.[11,13] Clearly, the headgroup plays an important role not only in the determination of the existence and structure of the standing-up phases but also in the structure, or absence thereof, of the lying-down phases. In particular, the observed dimerization of the fatty acid molecules in the lying-down phases[11,13] may cause a dimer of two molecules to behave as a single "molecule". The twice-stronger chain−chain attraction of this twice-longer "molecule" may induce the order formation in fatty acids on mercury. This view is supported by the fact that an increase in order with chain length is indeed found for the lying-down phases of fatty acids on mercury.[13] If this hypothesis is correct, then mercury-supported Langmuir films of alcohols of lengths considerably larger than those studied here may also exhibit long-range order in their lying-down phases. The details of the role of the headgroup are now being studied by us employing mercury-supported Langmuir films of a range of judiciously chosen molecules with various headgroups and molecular architectures.

3. Molecular Tilts. To detect possible small molecular tilts in the standing-up phases, we measured the BR at the GID peak positions for the alcohols studied. The results for the (11) diffraction peak at $T = 25$ °C and $q_{||} \approx 1.51$ Å^{-1} are summarized in Figure 10. For a better comparison all Bragg rods are scaled to have the same intensity of the Bragg rod under the sharp Vineyard peak[24] at $q_z \approx 0.06$ Å^{-1}. All BRs are observed to peak at $q_z \approx 0$ Å^{-1}. Fits to the BRs of C14OH, C22OH, and C26OH yield all tilt angles of less than 2° from the surface normal. Hence we conclude that within the accuracy of our measurements all phases are untilted for all the alcohols above. For C18OH, the shape of the BR curve, peaking somewhat above $q_z = 0$ Å^{-1}, indicates a small molecular tilt. The fitted tilt angle

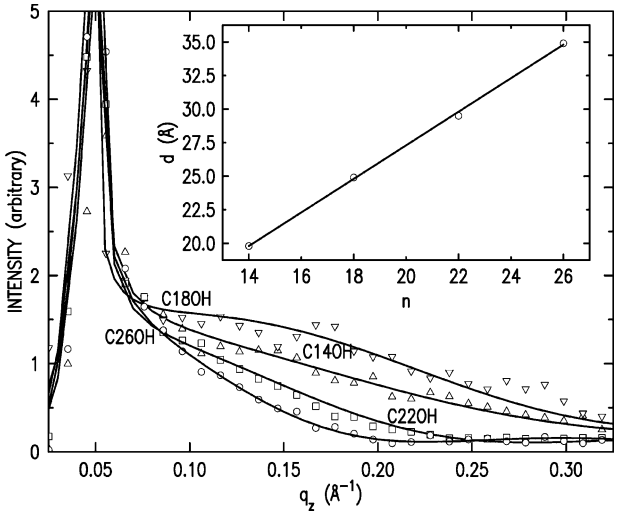

Figure 10. BR of the standing-up phases of C14OH, C18OH, C22OH, and C26OH at $T = 25$ °C. The BR of C18OH indicates a molecular tilt of $\varphi = 4.5°$ from the surface normal; the other molecules are untilted. The inset shows the layer thicknesses as obtained from the reflectivity curves. The linear behavior and its slope indicate negligible tilts for all molecular lengths.

is $\varphi = 4.5°$. This small tilt, not detectable in XR but only in BR measurements, is consistent with other studies of chain molecules in the LS phase. As shown in the inset, the reflectivity measurements show a linear dependence of the layer thickness d on chain length, with a linear fit yielding $d = (2.3 \pm 0.5) + (1.25 \pm 0.03)n$ Å, which coincides with the extended length of the molecules, within the quoted error bars. Thus, we can safely conclude that at the highest coverage the standing-up phases of alcohols on mercury are, in general, the same as those of alcohols on water. However, due to the considerably higher pressures in these phases on mercury ($\pi \geq 50$ mN/m) the tilted phases, observed on water ($\pi \leq 25$ m/m), are completely suppressed and only untilted phases are observed. At molecular areas A where tilted phases are observed on water, we observe on mercury a coexistence of a lying-down phase with an untilted standing-up phase.

C. Phase Diagram. The information obtained from the isotherm and the X-ray measurements can be used to construct a general (n, A, π) phase diagram for Langmuir films of alcohols on mercury, with the caveat that we only have X-ray measurements for $n = 14$, 18, 22, and 26. The projection of this 3D phase diagram on the (n, π) plane is shown in Figure 11 for $T = 23$ °C. For $n \leq 7$ no stable Langmuir film is obtained. This is manifested by the surface pressure remaining close to zero down to a molecular area of ≲20 Å^2/molecule, where stable films of other n reach their collapse pressure. For $8 \leq n \leq 12$ a single plateau is observed in the isotherm. The exclusion area obtained from fits of the isotherms to the Volmer equation indicates the growth of a single layer of molecules lying flat on the surface. The high slope regions in the (A, π) isotherms at their low A ends indicate a condensed monolayer of standing-up molecules. Thus the single plateau in this n range can be assigned to a coexistence region between the single layer of lying-down molecules and the monolayer of standing-up molecules. The surface pressure of the plateau rises linearly with n, similar to Langmuir films of alkanes[12] and fatty acids[13] on mercury.

For $14 \leq n \leq 18$ we observe two plateaus in the isotherm, which the X-ray reflectivity measurements reveal to be associated with the formation of a 9.1 Å thick double layer of lying-down molecules, and a coexistence region, respectively. Increasing the coverage further leads to the

(24) Vineyard, G. H. *Phys. Rev. B.* **1982**, *26*, 4146.

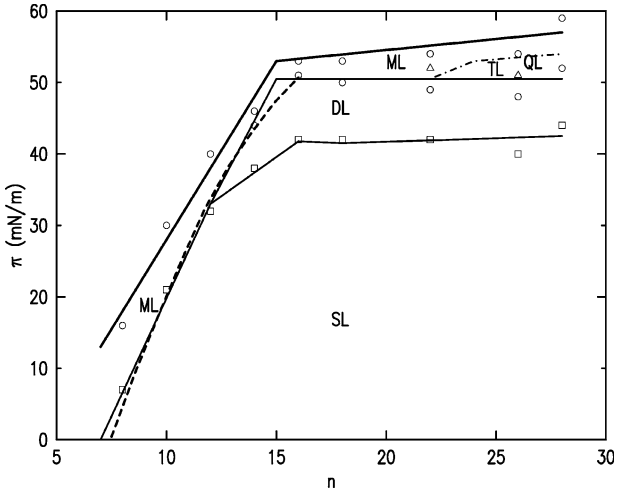

Figure 11. Surface pressure (π)−chain length (n) phase diagram for Langmuir films of alcohols on mercury at $T = 23$ °C. SL, DL, TL, and QL indicate single, double, triple, and quadruple layers of lying-down molecules. The dashed line is a fit of an expression, discussed in the text, yielding the adsorption energy of the alkyl chain and alcohol headgroup on mercury. ML indicates the monolayer phases of standing-up molecules. The various phases in this region are shown in Figures 8 and 9 and discussed in the related text. The solid uppermost line is the collapse pressure of the film.

formation of an untilted, hexagonally ordered, standing-up phase, of a structure identical with the LS phase of the same alcohols on water. The two alcohols investigated by X-rays in this n range, C14OH and C18OH, do not show any other standing-up phase within the 5−30 °C temperature range of our measurements for C14OH or at room temperature for C18OH.

For $22 \leq n \leq 26$ three plateaus are clearly observed in the isotherm, indicating three phases of flat-lying molecules: single, double, and triple layers. A very small additional plateau indicates in C26OH the formation of a quadruple layer of lying-down molecules, which is clearly observed by X-rays. This phase is not observed for any other chain lengths studied here. Interestingly, despite the three plateaus observed in the isotherm, C22OH shows in the X-ray measurements only the single- and double-layer phases of flat-lying molecules. The standing-up phases of these chain lengths were found to be the CS, S, or LS phases observed also on water.[1] Their boundaries and very existence were found to be temperature dependent. For the longest alcohol studied, C28OH, the number of plateaus decreases to two. This suggests the existence of only two lying-down phases: the single layer and the double layer.

All lying-down phases are found to lack long-range order in the surface-parallel direction. This includes the triple- and quadruple-layer phases where the closer packing of the multilayer structure, manifested in the lower layer spacing, could have been expected to induce a higher order than that in the single- and double-layer phases. This absence of long-range in-plane order is in contrast with its presence in the lying-down phases of fatty acids on mercury[13] but in line with the absence of order also in alkanes on mercury.[12] The difference clearly originates in the different interactions between the main order-inducing agents in the lying-down phases: the headgroups.

As we have done previously for alkanes[12] and fatty acids,[13] we can extract from the phase boundaries an estimate for the adsorption energies on mercury of the alkyl chain and alcohol headgroup. This is done by viewing the surface pressure π, to a first approximation, as being equal to the difference between the adsorption energy E_{ads} and the heat of vaporization ΔH_{vap}. The simple theoretical expression obtained[12] is fitted to the surface pressure of the first plateau. The fit is shown in a dash line in Figure 11. It yields adsorption energies of 4.9 kJ/(CH_2 mol) for a methyl group and $E_{ads} \approx 21$ kJ/(CHOH mol) for the alcohol headgroup. The result for a methyl group agrees very well with the 5.4 kJ/(CH_2 mol) obtained from alkanes on mercury[12] and the 5.3 kJ/(CH_2 mol) obtained for fatty acids on mercury.[13] The alcohol headgroup's adsorption energy is about 25% smaller than the $E_{ads} \approx 28$ kJ/(CHOOH mol) of the fatty acid headgroup.

This simple calculation shows that the energetics favor lying-down phases at low coverage, since this maximizes the total adsorption energy. The transition to a standing-up phase requires raising the pressure by increasing the coverage. It also explains why the lying-down phases disappear for short molecules; with decreasing n the energetic advantage in maximizing the alkyl−mercury contact by having a lying-down phase diminish relative to that of maximizing the headgroup−mercury contact by having a standing-up phase. Finally, the coverage at which the transition from lying-down to standing-up phases occurs depends sensitively on the balance between the mercury−alkyl and mercury−headgroup interaction, and the variation of this balance with pressure. When the later interaction strength decreases the transition point is shifted toward higher coverages and pressures. This, in turn, results in the formation of a larger number of lying-down layers before these are preempted by the transition from lying-down to standing-up molecules. Thus, for alcohols, where E_{ads} is lower (as compared to fatty acids), even quadruple layers of lying-down molecules can be observed before the formation of additional lying-down layers is preempted by the transition to standing-up molecules. By contrast, for fatty acids, where the headgroup's E_{ads} is higher, only single and double layers of flat-lying molecules are observed.

V. Conclusions

Langmuir films of alcohols on mercury are found to have, in general, a similar phase behavior to that of fatty acids on mercury.[13] However, a number of important differences should be noted. The most prominent of these is that the lying-down phases of alcohols do not show long-range order, while those of fatty acids are ordered. This is due most probably to the stronger headgroup−headgroup and headgroup−mercury affinities for fatty acids as compared to alcohols. Also, the tilted standing-up phases, observed on water for fatty acids and alcohols, and in a suppressed form also for fatty acids on mercury, are completely suppressed here, and only untilted standing-up phases are observed for alcohols on mercury, excepting C18OH, where a minute tilt of 4.5° is observed. This can be explained by the larger number of layers of lying-down molecules occurring for the long chain alcohols. This increases the surface pressure and decreases significantly the possibility of forming a coexisting tilted standing-up phase, which requires more surface area per molecule than an untilted phase. The suppression of tilted phases for fatty acids on mercury and the total lack of these phases for alcohols on mercury are consistent with the observed surface pressures at the transitions to the untilted standing-up phases on mercury and water. For Langmuir films of fatty acids, we observe at the transition point to the untilted phases a pressure of $\pi \approx 45$ mN/m on mercury and $\pi \approx 30$ mN/m on water. For alcohols, however, the corresponding pressures are $\pi \approx 50$ mN/m on mercury and $\pi \approx 20-25$ mN/m on water.[25,26] The

pressure gap $\Delta\pi$ for alcohols is almost twice larger than that of fatty acids. This leads to a complete suppression of tilted phases for alcohols on mercury. Further studies, in particular with headgroups having both stronger and weaker interactions with the mercury subphase, should provide deeper insight into the interactions dominating the topology of the phase diagram of Langmuir films of chain molecules on mercury.

Acknowledgment. Support to M.D. by the U.S.−Israel Binational Science Foundation, Jerusalem, and to P.S.P. by the NSF (Grant No. DMR-0124936) is gratefully acknowledged. BNL is supported by U.S. DOE Contract No. DE-AC02-98CH10886.

LA0497954

(25) Shih, M. C.; Durbin, M. K.; Mali, A.; Zschack, P.; Dutta, P. *J. Chem. Phys.* **1994**, *101*, 9132.
(26) Fischer, B.; Teer, E.; Knobler, C. M. *J. Chem. Phys.* **1995**, *103*, 2365.